

Mechanism for direct conversion of graphite to diamond

Jian-Tao Wang,^{1,2,*} Changfeng Chen,² and Yoshiyuki Kawazoe³

¹Beijing National Laboratory for Condensed Matter Physics, Institute of Physics, Chinese Academy of Sciences, Beijing 100190, China

²Department of Physics and High Pressure Science and Engineering Center, University of Nevada, Las Vegas, Nevada 89154, USA

³Institute for Materials Research, Tohoku University, Sendai 980-8577, Japan

(Received 12 April 2011; revised manuscript received 25 June 2011; published 27 July 2011)

The atomistic mechanism for direct conversion of graphite to diamond is a long-standing problem in condensed matter physics. Here, we establish by *ab initio* calculations bond reconstruction pathways from graphite to a basic series of diamond polytypes of 2H, 3C, 4H, and 12R. The conversion proceeds through two newly identified compressed-graphite phases of orthorhombic and monoclinic carbon with odd-membered (5 + 7) rings toward the diamond structures via a local-bond-rotation mechanism. The rhombohedral 12R phase represents a new crystal form of diamond with an alternating four-layered hexagonal (h) and cubic (c) close-packed structure in (hcch)₃ stacking. These results resolve the fundamental questions about the graphite-to-diamond phase transformation at high pressure and high temperature.

DOI: [10.1103/PhysRevB.84.012102](https://doi.org/10.1103/PhysRevB.84.012102)

PACS number(s): 61.50.Ks, 62.50.-p, 64.60.My, 71.15.Mb

Direct conversion of graphite to diamond is among the best-known structural phase transformations in condensed matter physics, but its underlying mechanism has remained enigmatic despite decades of experimental and theoretical exploration. Diamond has been synthesized by direct conversion of graphite at high pressure above ~ 13 GPa and high temperature above ~ 1300 K using a multianvil apparatus.^{1–5} Beside hexagonal and cubic diamond, an unquenchable transparent and hard phase has been observed under cold compression of graphite at room temperature.^{6–11} It reverts to graphite with release of pressure at room temperature,^{5–9} but transforms to diamond^{5–7} with *in situ* heating under pressure. Numerous studies have explored its structural characteristics.^{5–8} Recent x-ray diffraction (XRD) results⁸ constrain its symmetry to orthorhombic and monoclinic. This has led to the latest theoretical identification of two structural forms for compressed graphite, a monoclinic *M* carbon¹² and an orthorhombic *W* carbon.¹³ These newly identified structures provide a crucial link for resolving the long-standing problem of understanding the graphite-to-diamond phase transformation at high pressure and high temperature.

In this Brief Report, we present a comprehensive study of the energetics and kinetics of direct phase conversion from graphite to diamond via the intermediate phases of orthorhombic *W* and monoclinic *M* carbon under a wide pressure range of 5–25 GPa. We identify by *ab initio* calculations a basic series of diamond polytypes of 2H, 3C, 4H, and 12R transformed from the *W* and *M* carbon with a novel local-bond-rotation reconstruction mechanism from metastable odd-membered-ring (5 + 7) structures in *M* and *W* carbon toward stable even-membered-ring (6 + 6) diamond structures. We demonstrate that *M* carbon can easily transform to hexagonal (2H) diamond with a relatively small barrier of 0.33 eV, while *W* carbon favors transformation to rhombohedral 12R diamond with a barrier of 0.39 eV. Meanwhile, phase conversion from hexagonal 2H to cubic 3C diamond would encounter a larger barrier of 0.49 eV. The rhombohedral 12R phase predicted by the present work represents a new crystal form of diamond in $R\bar{3}m$ symmetry, comprising an alternating four-layered hexagonal (h) and cubic (c) diamond in (hcch)₃ stacking.

The calculations are carried out using density functional theory within the local density approximation (LDA) as implemented in the Vienna *ab initio* simulation package.¹⁴ The all-electron projector augmented wave method¹⁵ was adopted with $2s^22p^2$ treated as valence electrons. A plane-wave basis set with an energy cutoff of 800 eV was used and gave well converged total energies of ~ 1 meV/atom. Forces on the ions are calculated through the Hellmann-Feynman theorem allowing a full geometry optimization. The phase transitions are simulated using the climbing image nudged elastic band (CI NEB) method.¹⁶

Experimentally, direct conversion of graphite to diamond under static pressure without any catalysts or solvents is conducted by a two-stage process: pressure is increased first over several hours up to 12–25 GPa, and then temperature is increased up to 2000–2800 K within 20–30 min.¹⁷ As revealed by recent studies,^{12,13} under cold compression graphite turns into *M* carbon¹² and *W* carbon¹³ phases, which can be regarded as distorted graphite in an ABAB stacking, as in the well-known (2 × 1) reconstruction of the (111) surface of diamond and silicon.¹⁸ However, the odd-membered-ring (5 + 7) structure (see Fig. 1) in bulk structure here is unstable and has a tendency of transforming to the most stable sp^3 even-membered-ring (6 + 6) diamond structure with a remarkable energy gain of 0.18 eV per atom.

To probe the underlying atomistic mechanism of the phase transformation, we examine several possible structures and pathways toward the formation of diamond phases with various *local-bond-rotation reconstruction* process from odd-membered-ring (5 + 7) structure in *M* and *W* carbon toward even-membered-ring (6 + 6) structure in diamond polytypes. Starting from *W* carbon, two possible diamond polytypes of 12R and 4H are identified [Figs. 1(a) and 1(b)]. The 12R phase can be formed by the selective change of the armchair buckling [A₁(2,3)A₂(2,3)] or [A₁(1,4)A₂(1,4)]; 4H can be formed by the change of the armchair buckling [A₁(1,4)A₂(2,3)] or [A₁(2,3)A₂(1,4)]. By the same process, starting from *M* carbon, three possible diamond polytypes of 2H, 12R, and 3C are identified [Figs. 1(c)–1(e)]. The 2H phase can be obtained via the buckling change of [A₁(2,3)A₂(2,3)]; 12R can be obtained via the buckling change of [A₁(1,4)A₂(2,3)]

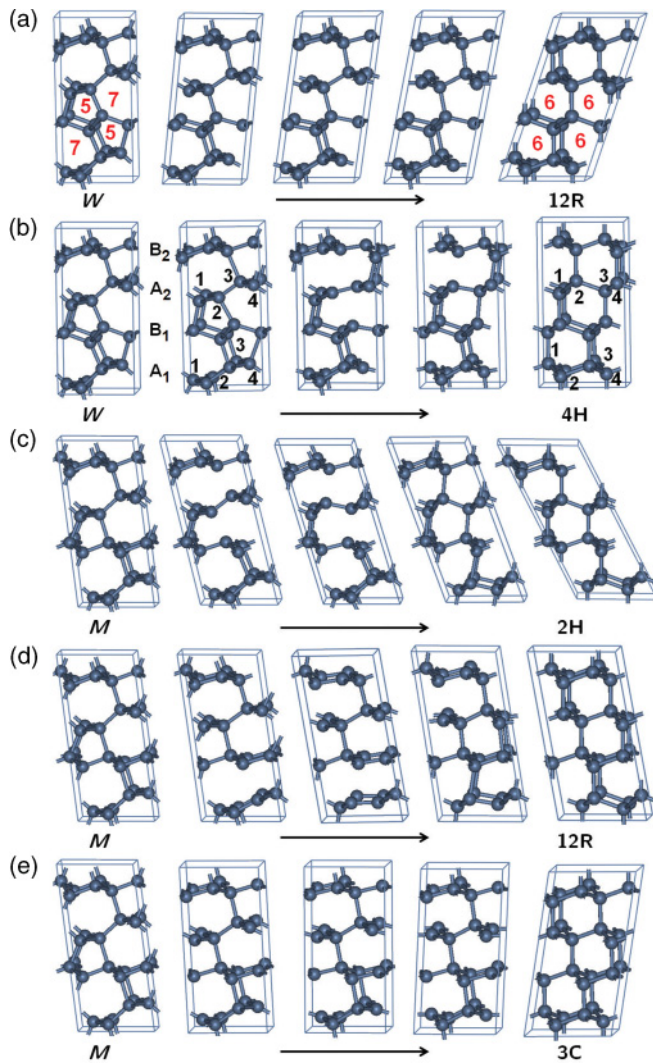


FIG. 1. (Color online) Geometries and pathways to form 2H, 4H, 3C, and 12R diamond from orthonrhombic W and monoclinic M carbon with distinct local-bond-rotation and deformation reconstruction mechanisms from metastable odd-membered-ring (5 + 7) structure in M and W carbon toward stable even-membered-ring (6 + 6) diamond structures.

or $[A_1(2,3)A_2(1,4)]$; and 3C can be obtained via the buckling change of $[A_1(1,4)A_2(1,4)]$. Moreover, throughout the pathways $W \rightarrow 12R$, $M \rightarrow 2H$, and $M \rightarrow 3C$, a lattice deformation accompanies the *local-bond-rotation reconstruction* process. In all, four basic diamond polytypes of 2H, 3C, 4H, and 12R are identified starting from the intermediate cold-compressed graphite phases of W and M carbon.

Figure 2 shows the enthalpy along the pathways toward the formation of 12R, 4H, and 3C from W carbon, and 2H, 12R and 3C from M carbon at 15 GPa. These pathways are simulated using the CI NEB method¹⁶ with a 16-atom supercell containing four carbon sheets. No symmetry constraint was imposed in the structural optimization procedure. One can see that W carbon favors transformation to rhombohedral 12R diamond with a barrier of 0.39 eV, and to 4H diamond with a relatively larger barrier of 0.43 eV. For comparison, we also show a pathway for W carbon to 3C via a sliding model

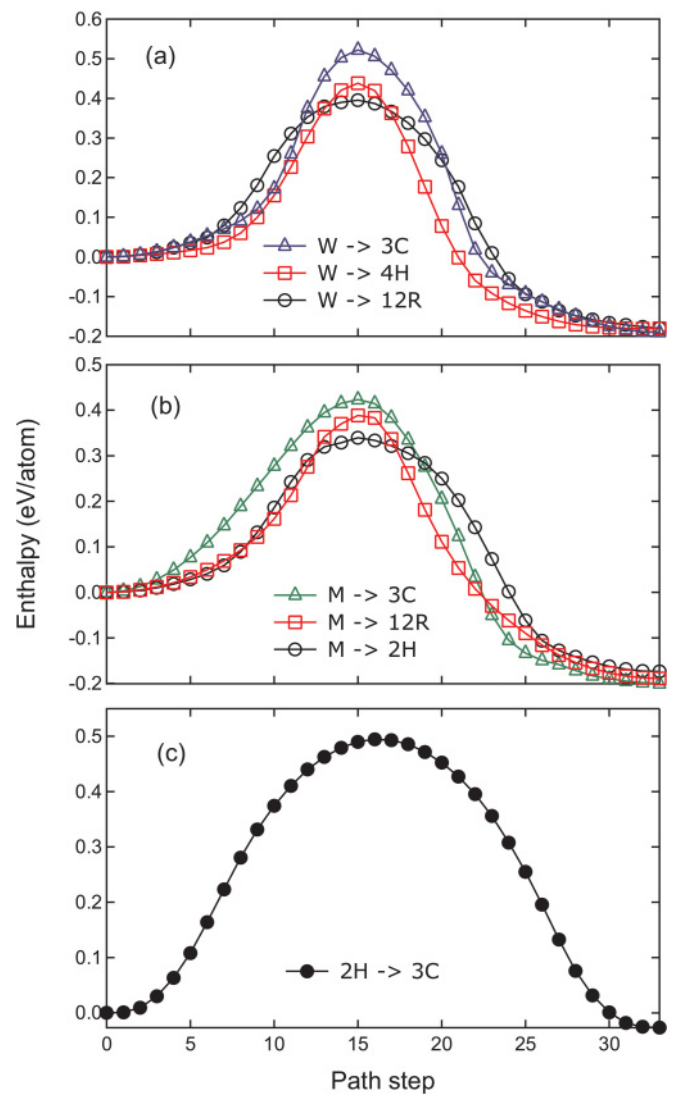


FIG. 2. (Color online) Enthalpy versus pathway for phase conversions at 15 GPa. (a) $W \rightarrow 12R$, 4H, 3C; (b) $M \rightarrow 2H$, 12R, 3C; (c) $2H \rightarrow 3C$. The pathways are shown in Fig. 1.

(B_1 layer in Fig. 1), which results in a higher barrier of 0.52 eV. It is observed that for phase conversions between the dense, hard phases, local-bond-rotation processes are favored. Based on such processes, the barriers for transformations from M to 2H, 12R, and 3C are estimated to be 0.34, 0.38, and 0.42 eV, respectively. Among the local-bond-rotation processes, the pathways $W \rightarrow 12R$ and $M \rightarrow 2H$ with lattice deformation are more favored than others. Following a similar process, the barrier for the transformation from 2H to 3C is estimated to be 0.48 eV/atom [see Fig. 2(c)]. Similar barriers are also obtained for transformation from 12R and 4H to 3C.¹⁹

To illustrate the key role of pressure in various phase transformation processes shown above, we plot the relative enthalpy and enthalpy barriers versus pressure over a wide pressure range up to 25 GPa in Fig. 3. It is seen that pressure plays a dual role in lowering the conversion barrier and enhancing the production stability during the first-stage cold-compressed phase conversion of hexagonal

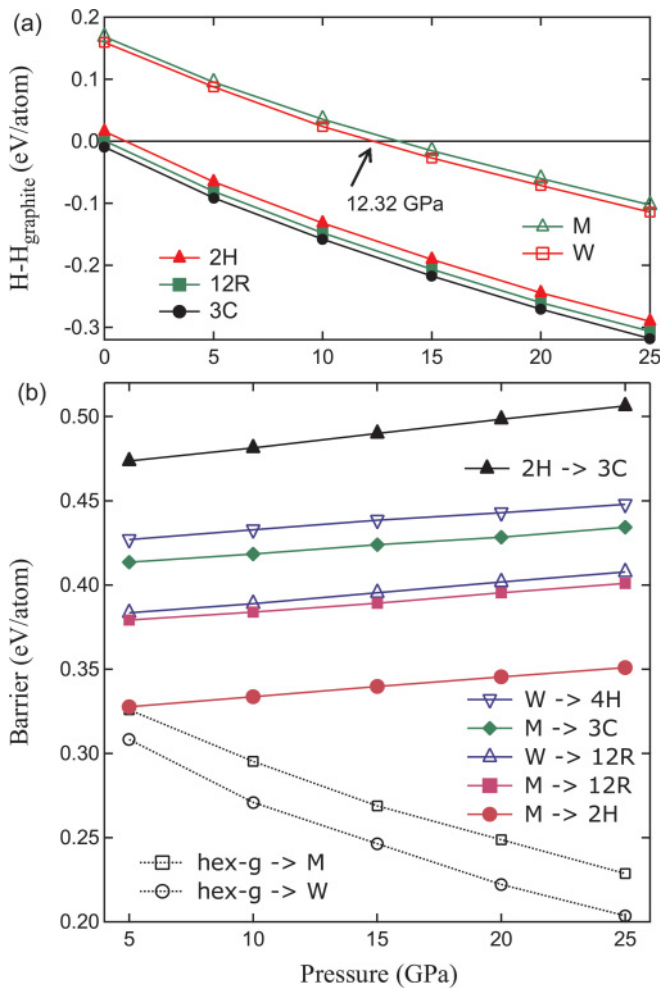


FIG. 3. (Color online) (a) The enthalpy per atom for 2H, 12R, 3C, M , and W carbon as a function of pressure relative to graphite. (b) Enthalpy barriers versus pressure. The barriers for hex-g \rightarrow M and hex-g \rightarrow W (Ref. 13) are also shown for comparison.

graphite (hex-g) toward the M and W phases; but it has little effect on the relative enthalpy and conversion barrier during the second-stage conversion process toward the diamond polytypes. It means that phase conversions between dense phases are dominated by temperature, which explains why high temperature is required diamond synthesis. Experimentally, the unquenchable transparent hard phases (W and M carbon) were observed under cold compression of graphite at room temperature and high pressure above ~ 13 GPa;^{6–11} hexagonal 2H diamond was obtained at high temperatures above ~ 1300 K;⁵ at further increased temperatures above ~ 2000 K, only cubic 3C diamond was observed in the run products.¹⁷ All these experimental findings can be described by our enthalpy barrier results: high pressure at room temperature facilitates the first-stage conversion hex-g \rightarrow M , W ; initial heating generates high-temperature and high-pressure conditions needed for the second-stage conversions $M \rightarrow 2H$ and $M, W \rightarrow 12R$; finally, further increased temperature leads to the third-stage conversion $2H \rightarrow 3C$. These results establish a new, multi-stage phase transformation mechanism via M and W carbon toward diamond polytypes.

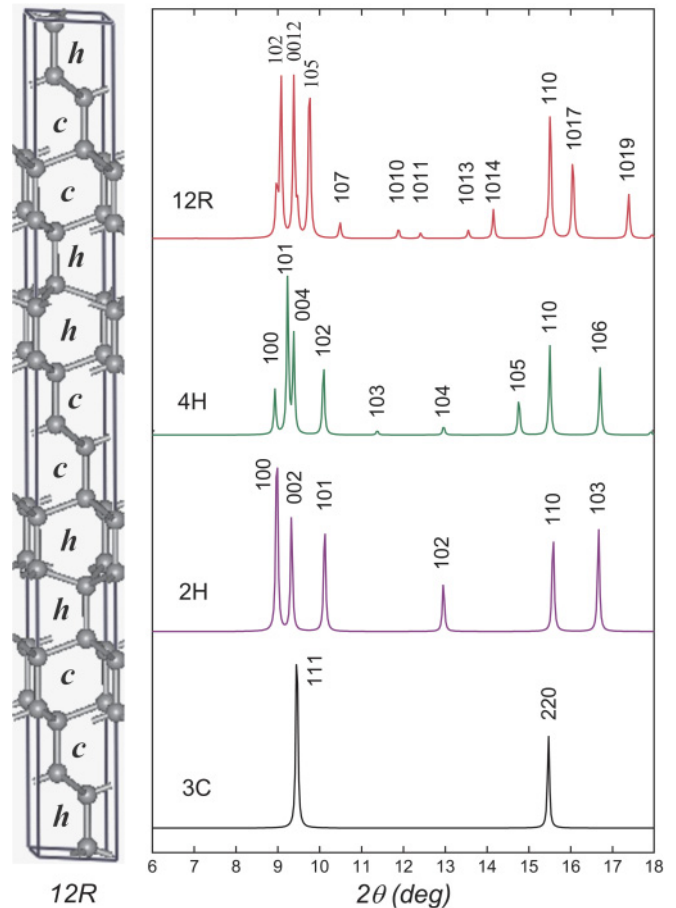


FIG. 4. (Color online) (Left) The hexagonal unit cell of 12R diamond. Symbols h and c denote hexagonal and cubic layers, respectively. (Right) Simulated XRD patterns of 12R, 4H, 2H, and 3C diamond at 15 GPa. X-ray wavelength is 0.3329 Å.

A large variety of diamond polytypes of 2H, 3C, 4H, 6H, 8H, 9R, 15R, and 21R have been reported both theoretically and experimentally.^{20–28} However, only 2H and 3C diamond have been synthesized and confirmed in bulk form, while all other diamond polytypes are obtained by chemical vapor deposition and are in mixed phase due to their similar energetic states. For example, 2H, 3C, and 9R diamond can coexist on silicon surface.²⁷ Our results establish a basic series of diamond polytypes of 2H, 3C, 4H, and 12R for bulk phase conversion. Note also that earlier theoretical work²⁹ has found that graphite under pressure transforms into a mixture of cubic and hexagonal diamonds, reminiscent of the rhombohedral 12R phase reported here.

The predicted 12R phase represents a new crystal form of diamond, which is only about 10 meV/atom higher in energy than 3C diamond, while lower in energy (15 meV/atom) than 2H diamond and close to 4H diamond [see Fig. 3(a)]. The 12R structure is closely related to both the cubic and hexagonal close-packed structures with a stacking fault occurring every four layers (see Fig. 1). The sequence repeats every 12 layers and the structure has rhombohedral symmetry in $(hcch)_3$ stacking, as in ZnS polytypes.³⁰ Its crystal structure with the space group $R\bar{3}m$ (D_{3d}^5) in hexagonal unit cell is shown in Fig. 4. At zero pressure, the equilibrium lattice parameters

TABLE I. Calculated equilibrium volume (V_0 in $\text{\AA}^3/\text{atom}$), bulk modulus (B_0 in GPa), and band gaps (E_g in eV) for diamond polytypes of 12R, 4H, 2H, and 3C at zero pressure, compared to available experimental and calculated data.

Structure	Method	V_0 (\AA^3)	B_0 (GPa)	E_g (eV)
12R	This work	5.53	474.6	4.50
4H	This work	5.53	470.1	4.59
2H	This work	5.53	466.7	3.13
3C	This work	5.52	466.3	4.20
	LDA (Ref. 12)	5.52	468.5	
	LDA (Ref. 31)			4.17
	Exp (Ref. 32)	5.67	446	5.47

are $a = 2.4908 \text{ \AA}$, $c = 24.6501 \text{ \AA}$, and $\gamma = 120^\circ$ with four inequivalent crystallographic sites, occupying the 6c (0.3333, 0.6667, 0.0733), (0.3333, 0.6667, 0.9058), (0.3333, 0.6667, 0.8437), and (0.6667, 0.3333, 0.9895) positions, respectively. The calculated density of 3.53 g/cm^3 is similar to that of both hexagonal and cubic diamond. By fitting the calculated total energy as a function of volume to the third-order Birch-Murnaghan equation, we obtain the bulk modulus (B_0) of 12R as 474.6 GPa, which is very close to the value for diamond (466 GPa). The LDA band gap is 4.50–4.42 eV over a wide pressure range of 0–25 GPa, which is remarkably larger than the value of 3.13 eV for 2H and even appreciably larger than the LDA gap (4.17 eV) (Ref. 31) for diamond. The calculated volume, bulk modulus, and band gaps at zero pressure are listed in Table I and compared to available experimental data for diamond.³²

Our results suggest that the phenomenon of polytypism may be an important consideration in the interpretation of powder XRD data of the different phases of carbon at

various temperatures as there are apparently only small energy differences between different polytypes. Figure 4 shows the simulated XRD patterns of 12R, 4H, 2H, and 3C diamond. With the change of structural symmetry from 3C to 12R form, the main peak $c(111)$ is split into more than three peaks. There are three strongest peaks at 9.08° (99%), 9.38° (100%), and 9.77° (86%) for 12R. The main peak at 9.38° is located and close to the $c(111)$ of 3C diamond. Experimental XRD patterns have shown two peaks overlap with $c(111)$ on both sides⁷ at 20 GPa and 1300 K, which could be the evidence that 12R diamond coexist with 3C diamond during the high-temperature phase conversion. Close scrutiny of more experimental data may reveal additional insights into the multiphase coexistence of diamond polytypes obtained under various synthesis conditions.

In summary, we have studied direct conversion of graphite to diamond using *ab initio* calculations. Our results reveal a basic series of diamond polytypes of 2H, 3C, 4H, and 12R transformed via intermediate compressed-graphite phases with distinct local-bond-rotation reconstruction mechanisms. The predicted rhombohedral 12R phase represents a new crystal form of diamond in (hcch)₃ stacking. These results resolve the fundamental questions about high-temperature and high-pressure phase transformation of graphite to diamond.

This study was supported by the NSFC of China (Grant No. 10974230) and CAS (Grant No. KJCX2-YW-W22). C.F.C. acknowledges support by DOE under Cooperative Agreement DE-FC52-06NA27684. Acknowledgment goes to the CREST project headed by M. Kotani for the support. We are thankful to the crew of the Center for Computational Materials Science at IMR, Tohoku University for their support at the SR11000 supercomputing facilities.

*wjt@aphy.iphy.ac.cn

¹R. B. Aust and H. G. Drickamer, *Science* **140**, 817 (1963).

²R. Clarke and C. Uher, *Adv. Phys.* **33**, 469 (1984).

³T. Irifune, A. Kurio, S. Sakamoto, T. Inoue, and H. Sumiya, *Nature (London)* **421**, 599 (2003).

⁴H. Sumiya and T. Irifune, *J. Mater. Res.* **22**, 2345 (2007).

⁵F. P. Bundy and J. S. Kasper, *J. Chem. Phys.* **46**, 3437 (1967).

⁶T. Yagi, W. Utsumi, M. A. Yamakata, T. Kikegawa, and O. Shimomura, *Phys. Rev. B* **46**, 6031 (1992).

⁷S. Endo, N. Idani, R. Oshima, K. J. Takano, and M. Wakatsuki, *Phys. Rev. B* **49**, 22 (1994).

⁸W. L. Mao, H. K. Mao, P. J. Eng, T. P. Trainor, M. Newville, C. C. Kao, D. L. Heinz, J. F. Shu, Y. Meng, and R. J. Hemley, *Science* **302**, 425 (2003).

⁹E. D. Miller, D. C. Nesting, and J. V. Badding, *Chem. Mater.* **9**, 18 (1997).

¹⁰W. Utsumi and T. Yagi, *Science* **252**, 1542 (1991).

¹¹Y. X. Zhao and I. L. Spain, *Phys. Rev. B* **40**, 993 (1989).

¹²Q. Li, Y. M. Ma, A. R. Oganov, H. B. Wang, H. Wang, Y. Xu, T. Cui, H. K. Mao, and G. T. Zou, *Phys. Rev. Lett.* **102**, 175506 (2009).

¹³J. T. Wang, C. F. Chen, and Y. Kawazoe, *Phys. Rev. Lett.* **106**, 075501 (2011).

¹⁴G. Kresse and J. Furthmüller, *Phys. Rev. B* **54**, 11169 (1996); G. Kresse and J. Hafner, *ibid.* **47**, 558 (1993).

¹⁵P. E. Blöchl, *Phys. Rev. B* **50**, 17953 (1994); G. Kresse and D. Joubert, *ibid.* **59**, 1758 (1999).

¹⁶See [<http://theory.cm.utexas.edu/henkelman>] for study of the kinetic processes at the atomic scale.

¹⁷T. Irifune, A. Kurio, S. Sakamoto, T. Inoue, H. Sumiya, and K. Funakoshi, *Phys. Earth Planet. Inter.* **143–144**, 593 (2004).

¹⁸K. C. Pandey, *Phys. Rev. Lett.* **47**, 1913 (1981).

¹⁹The gibbs free energy $G(T, P)$ can be written as $G(T, P) = E(V) + F_{ph}(T, V) + PV = H(P, V) + F_{ph}(T, V)$. The temperature T appears in $F_{ph}(T, V)$ via the phonon term only, which can induce a small volume expansion to affect the magnitude of the estimated barriers.

²⁰B. Wen, J. J. Zhao, M. J. Bucknum, P. K. Yao, and T. J. Li, *Diam. Relat. Mater.* **17**, 356 (2008).

²¹P. D. Ownby, X. Yang, and J. Liu, *J. Am. Ceram. Soc.* **75**, 1876 (1992).

²²F. P. Bundy, H. T. Hall, H. M. Strong, and R. H. Wentorf, *Nature* **176**, 51 (1955).

- ²³R. E. Hanneman, H. M. Strong, and F. P. Bundy, *Science* **155**, 995 (1967).
- ²⁴S. Welz, M. J. McNallan, and Y. Gogotsi, *J. Mater. Process. Technol.* **179**, 11 (2006).
- ²⁵S. Bhargava, H. D. Bist, S. Sahli, M. Aslam, and H. B. Tripathi, *Appl. Phys. Lett.* **67**, 1706 (1995).
- ²⁶Z. W. Wang, Y. S. Zhao, C. S. Zha, Q. Xue, R. T. Downs, R. G. Duan, R. Caracas, and X. Z. Liao, *Adv. Mater.* **20**, 3303 (2008).
- ²⁷Y. Lifshitz, X. F. Duan, N. G. Shang, Q. Li, L. Wan, I. Bello, and S. T. Lee, *Nature* **412**, 404 (2001).
- ²⁸R. Kapil, B. R. Mehta, and V. D. Vankar, *Appl. Phys. Lett.* **68**, 2520 (1996).
- ²⁹S. Scandolo, M. Bernasconi, G. L. Chiarotti, P. Focher, and E. Tosatti, *Phys. Rev. Lett.* **74**, 4015 (1995).
- ³⁰S. Haussühl and G. Müller, *Miner. Petrog. Mitt.* **9**, 28 (1963).
- ³¹W. G. Aulbur, M. Stadelé, and A. Gorling, *Phys. Rev. B* **62**, 7121 (2000).
- ³²F. Occelli, P. Loubeyre, and R. Letoullec, *Nat. Mater.* **2**, 151 (2003).